Krunoslav Haramina
Nenad Kranjčević
Matija Hoić ✉
Joško Deur
Andreas Tissot

https://doi.org/10.21278/TOF.483057923
ISSN 1333-1124
eISSN 1849-1391

MODELLING OF E-CLUTCH AXIAL DYNAMICS BASED ON EXPERIMENTALLY IDENTIFIED CLUTCH COMPONENT STRESS-STRAIN CHARACTERISTICS

Summary

E-clutch systems allow for a conventional or electrified powertrain control system to operate the transmission clutch for expanded functionalities, reduced fuel consumption, and improved driving comfort. To facilitate E-clutch control system design and enable its simulation verification, an accurate E-clutch model is required. The paper presents a lumped-parameter model of E-clutch axial dynamics parameterized based on experimentally identified stress-strain characteristics of individual components of a disassembled clutch. An initial, simplified model is first presented and parameterized based on the overall, input-output stress-strain characteristics identified. While the experimental validation results show that the initial model provides a satisfactory prediction of the clutch torque static curve, the prediction of the release bearing force static curve is less satisfactory, thus indicating a potential for further model improvements. Therefore, new, more detailed versions of the model containing individual component stress-strain characteristics are proposed and experimentally validated. The validation results indicate considerable improvements in the normal force static curve prediction accuracy when using the extended model.

Key words: *E-clutch, axial dynamics, experimental identification, modelling, validation*

1. Introduction

Manual transmission (MT) dry clutches can be actuated to combine the cost efficiency and fuel economy of MTs [[1][2][3]] with the driving comfort of a traditional automatic transmission [4]. The solution presented in [5] includes a clutch-by-wire system in combination with a manual gear shift transmission. In such a system, also known as an E-clutch, the clutch pedal is not mechanically connected to the clutch; instead, a position sensor is placed on the clutch pedal to provide a driver intention signal to the control system, which then operates the clutch by means of an actuator (see Fig. 1), [6][7]. In this way, the driver can maintain his typical MT driving habits while being assisted by the control system in reaching a better fuel

Abbreviations:	
CAN - Controller Area Network	IC - Internal Combustion
CSC - Clutch Slave Cylinder	LVDT - Linear Variable Differential Transformer
DMF - Dual Mass Flywheel	MC - Master Cylinder
HCA - Hydraulic Clutch Actuator	MT - Manual Transmission

economy in specific transmission operating modes and avoiding disturbing conditions such as engine stalling. An additional application of the E-clutch system is in hybrid electric vehicles, where it can allow for automated and efficient creep, coasting, and recuperation driving modes [7]. Although fully electric vehicles usually comprise a single-stage transmission, the application of clutch-based multi-speed transmissions is also investigated [8], particularly for commercial vehicles [9].

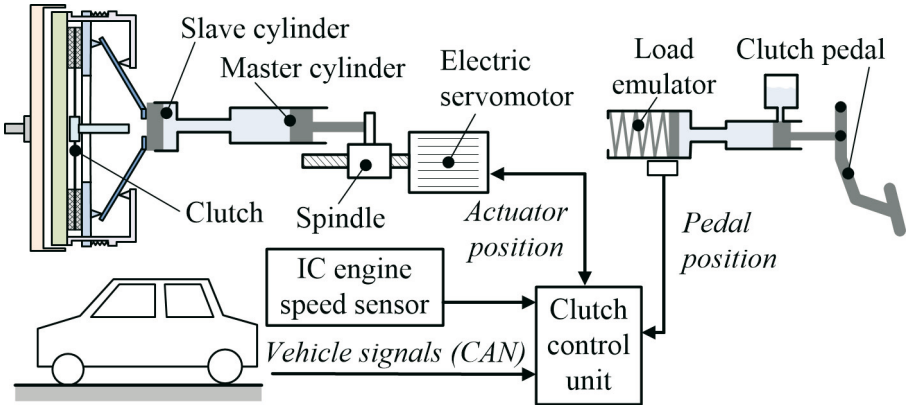

Fig. 1 Functional schematic of an E-clutch (clutch-by-wire) system with an electrically driven hydrostatic actuation system [15].

An accurate dry clutch model is beneficial in terms of gaining an understanding of clutch behaviour under static and dynamic conditions, designing the clutch itself [10], [11], and synthesising the clutch and transmission control systems, including simulation verification [12][13][14]. A model of the hydrostatic actuator dynamics, which has shown a good prediction quality for both static and dynamics conditions, as well as an initial model of the clutch axial dynamics were presented in [15]. Our paper extends the models presented in [15] in terms of giving more detailed models of clutch axial dynamics that can accurately predict not only the clutch torque static curve but also the static curves of other clutch variables, such as a release bearing force. The model is based on the stress-strain curves of individual clutch components that are experimentally identified by using a manually powered and instrumented spindle-based test rig.

The paper is organized as follows: the considered E-clutch system is described in Section 2; the previously developed actuator and initial clutch models are presented in Section 3, including the corresponding validation results.; Section 4 presents the newly developed clutch models; the parametrization of individual clutch model components is described in Section 5; the models are experimentally validated and assessed in Section 6, and concluding remarks are given in Section 7.

2. E-clutch system and test rig

2.1 Description of the E-clutch system

The E-clutch system considered comprises two distinctive (and mechanically separable) subsystems: a hydrostatic-type actuator driven by an electric servomotor and a traditional MT single-friction plate, normally closed dry clutch (see Fig. 2). The basic description of the E-clutch is given below, with reference to [15] and the literature given therein for more details.

The actuator itself can be divided into two subsystems: the hydraulic clutch actuator (HCA) and the clutch slave cylinder (CSC). The HCA unit is located on the outer surface of the clutch bell housing (see Fig. 4c). It includes three main components: an electrical servomotor of brushless DC type, a planetary spindle, and a primary hydraulic ("master") cylinder. The CSC unit is positioned on the transmission input axis, thus acting directly on the diaphragm spring (see Fig. 3a). The tube-like form enables the positioning of the CSC around the transmission input shaft. The following components form the CSC unit: the secondary ("slave") hydraulic cylinder, bleeding (safety) valve, release bearing, and the return spring. The HCA and CSC units are connected via a single hydraulic fluid pipeline. The HCA unit is equipped with a piston position, a motor voltage, and fluid pressure sensors, while the CSC unit contains an optional release bearing position sensor.

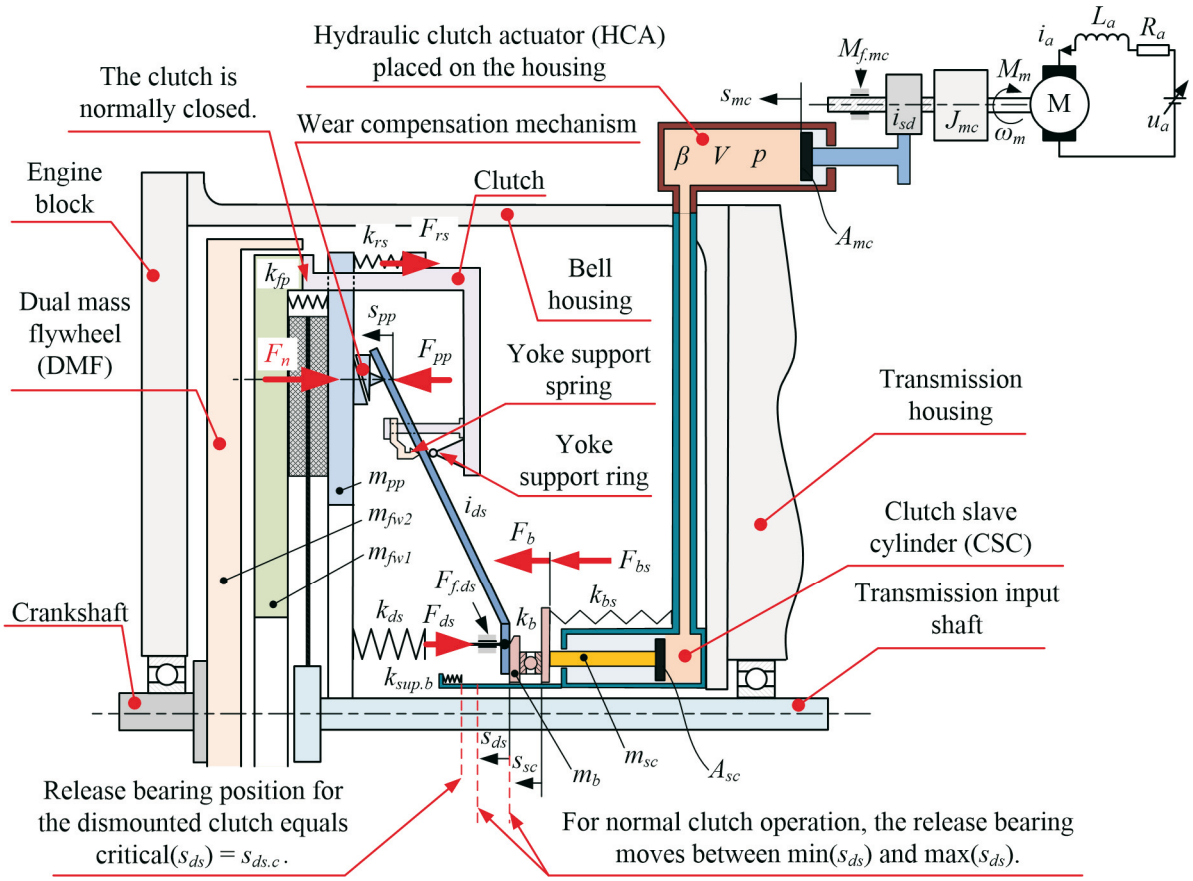

Fig. 2 Schematic of the E-clutch mechanism [15].

2.2 Test rig

The experimental work in [15] was initially focused on the actuator subsystem characterization by means of a test rig comprising the assembled actuator and the bell housing with a linear load spring replacing the actual clutch (see Fig. 3). A manual spindle mechanism

was used to generate preload on the CSC, equivalent to the load force of the clutch. The same manual press rig has been used in this study to identify the clutch component spring characteristics.

The main clutch test rig includes a driving servomotor, which transmits power via a telemetry torque sensor system to a dual-mass flywheel (DMF), and a clutch mounted in the original bell housing (Fig. 4a). The friction plate is mounted on the fixed transmission input shaft (i.e., the friction plate does not rotate; see Fig. 4d). The hydrostatic actuator and release bearing are mounted in the same way as on the real transmission (see Figs. 4b, 4c, and 4d).

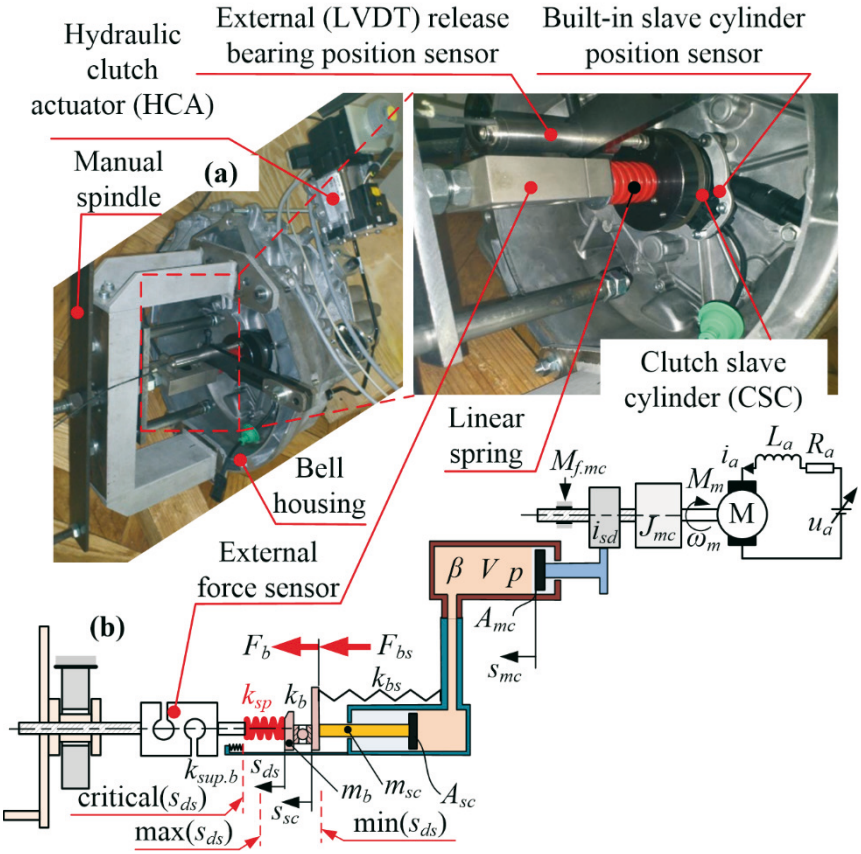

Fig. 3 E-clutch actuator test rig: (a) photographs and (b) structure schematic [15].

Five temperature sensors are installed on the clutch test rig. Three of them are installed in the pressure plate and in the primary and secondary flywheel discs; the fourth one is installed on the yoke and the fifth one is located on the outer surface of the bell housing. The sensor signals are transferred to the amplifiers by means of a precision slip-ring system. The primary and secondary discs of the DMF are fixed one to the other by means of six radially placed bolts to prevent damaging the temperature sensor wires during relative circular motion between the DMF discs. The measurement and control subsystems of the test rig are built around an industrial Pentium III PC, and the control software is written in the C programming language. More details on the design of the test rig can be found in [15] and [16].

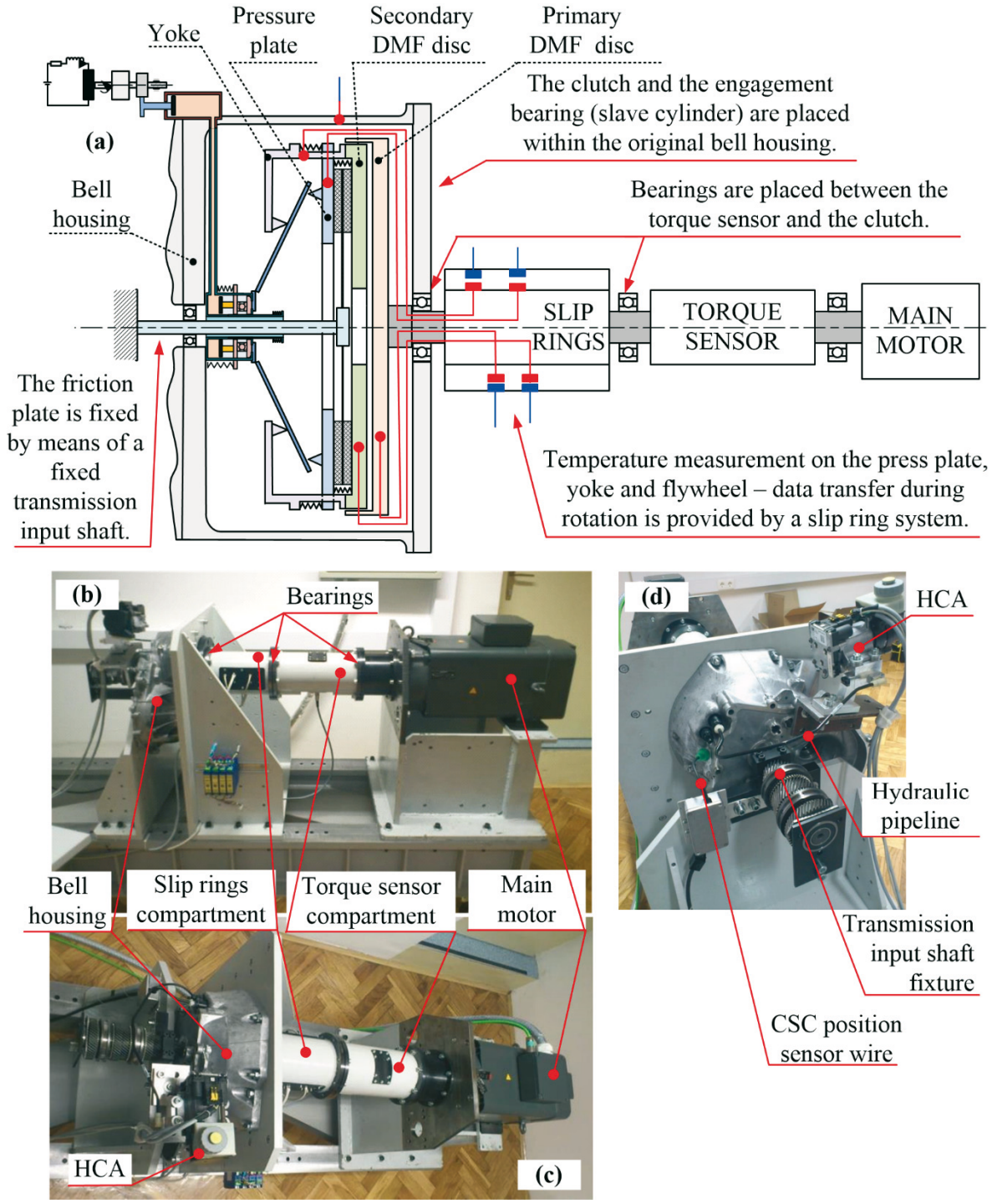

Fig. 4 Functional schematic and photographs of the E-clutch test rig [15].

3. The current bond graph model

3.1 Actuator model

The actuator model (Fig. 5a) has been developed in [15]. The model is represented by the bond graph shown in Fig. 5a, which follows the actuator structure presented in Fig. 3. The model is described in detail and experimentally validated in [15].

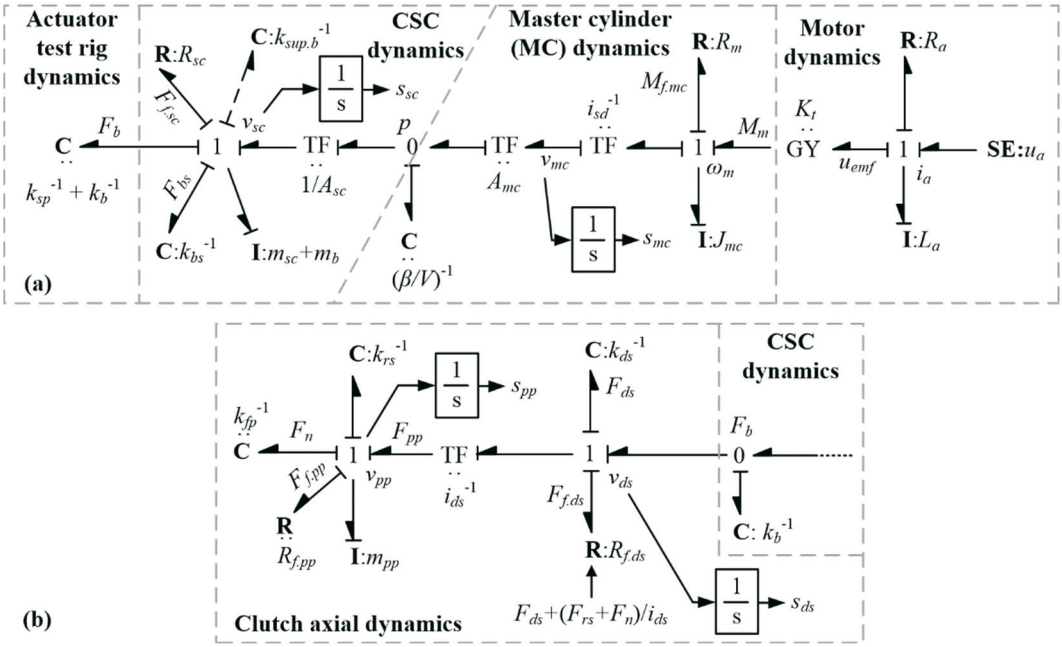

Fig. 5 Bond graph models of (a) the hydrostatic clutch actuator subsystem and (b) the clutch axial dynamics subsystem [15].

3.2 Clutch model 0

A model of crude control-oriented clutch axial dynamics (denoted here as Model 0; Fig. 5b) has been developed in [15]; it is connected to the actuator model via the release bearing stiffness (**C**: $1/k_b$) to match the input-output causalities of the two models.

The input part of the model describes the diaphragm spring dynamics through the diaphragm spring compliance (**C**: $1/k_{ds}$) and friction (**R**: $R_{f.ds}$). The output part of the model relates to the transfer of force from the diaphragm spring towards the pressure plate; it includes friction in the pressure plate (**R**: $R_{f.pp}$), an inertial force element **I**: m_{pp}, and the compliance of the return springs (**C**: $1/k_{rs}$) and the friction plate (**C**: $1/k_{fp}$). The transformation ratio between these two subsystems is described by the diaphragm spring lever transfer ratio (**TF**: $1/i_{ds}$; $i_{ds} < 0$). The clutch torque (M_{cl}) is calculated from the normal force (F_n), the effective friction plate radius (r_{eff}), and the coefficient of friction (μ, herein set to a constant value) as $M_{cl} = 2F_n\, r_{eff}\, \mu$, where the factor 2 accounts for two active friction surfaces (Fig. 4a). The parametrization of the model was based on the experimental determination of the stress-strain characteristics of the friction plate (k_{fp}) and fully assembled clutch [15].

3.3 Validation of the actuator and clutch model 0

The clutch actuator model shown in Fig. 5a has been validated successfully against experimental data recorded using the actuator test rig shown in Fig. 3 [15], as illustrated by the results shown in Fig. 6a.

Validation of the clutch axial dynamics model has been conducted for a new clutch at room temperature using data recoded on the main clutch test rig from Fig. 4. The validation results shown in Fig. 6b indicate a good qualitative correlation between the recorded and predicted clutch torque static curves. Quantitative accuracy can be ensured only when introducing additional compliance in the system (replacing the measured friction plate stiffness k_{fp} with $k_{fp}' < k_{fp}$ to account for the compliance of diaphragm spring levers, yoke support ring, and/or pressure plate; see Fig. 6). It may, thus, be concluded that more detailed characterization of individual clutch components as well as related first-principle model modifications are generally needed to ensure better modelling accuracy.

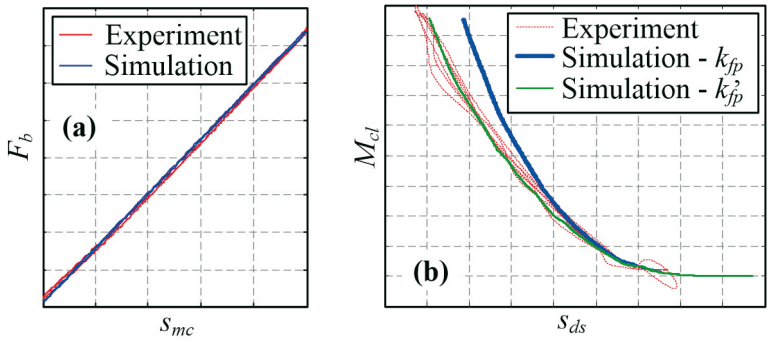

Fig. 6 Validation results of the (a) actuator and (b) clutch models [8].

4. A detailed characterization of clutch component compliance

Following the completion of clutch characterization experiments carried out on the full clutch test rig (Section 3), the clutch was disassembled, and the individual clutch components were experimentally characterized using the equipment and procedure previously used in [17].

A manually powered spindle-based press test rig (see Fig. 7) was used to experimentally determine the spring characteristics of individual components. Direct measurement of the normal force was obtained by placing an S-type force sensor (an HBM S-9 model with a measurement range of 10 kN) in between the spindle and the tested component. Direct measurement of the corresponding displacement was obtained by placing an LVDT position sensor (an Omega LD320-10 model with a +/- 10 mm range) in parallel to the force sensor. An additional LVDT position sensor (an Inelta Sensorsysteme IKAT5 model with a +/- 2.5 mm range) is used for either (i) the measurement of other relevant points on the same component or (ii) the verification of the main LVDT sensor. All the data were recorded by means of a PC-based data acquisition system, where the analogue signals from the sensors were transferred to a digital signal by means of a plug-in data acquisition card.

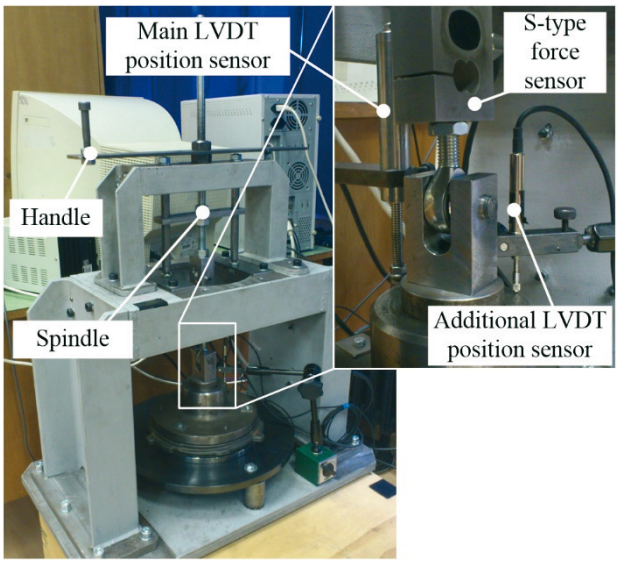

Fig. 7 Photographs of a manual press test rig.

Figure 8 shows photographs of individual clutch components mounted on the manual press test rig. The corresponding, experimentally recorded stress-strain static curves are shown in Fig. 9. It should be noted that the plots in Fig. 9 have different axis scales due to significantly different maximum displacements of individual components for the same force input.

Typically, raw experimental results (blue plots) exhibit a relatively narrow hysteresis because of friction between individual components, which can successfully be removed by averaging the recorded curves (black lines). The averaged values over three repeated experiments or cycles (green lines) are used as a final characteristic of the given component.

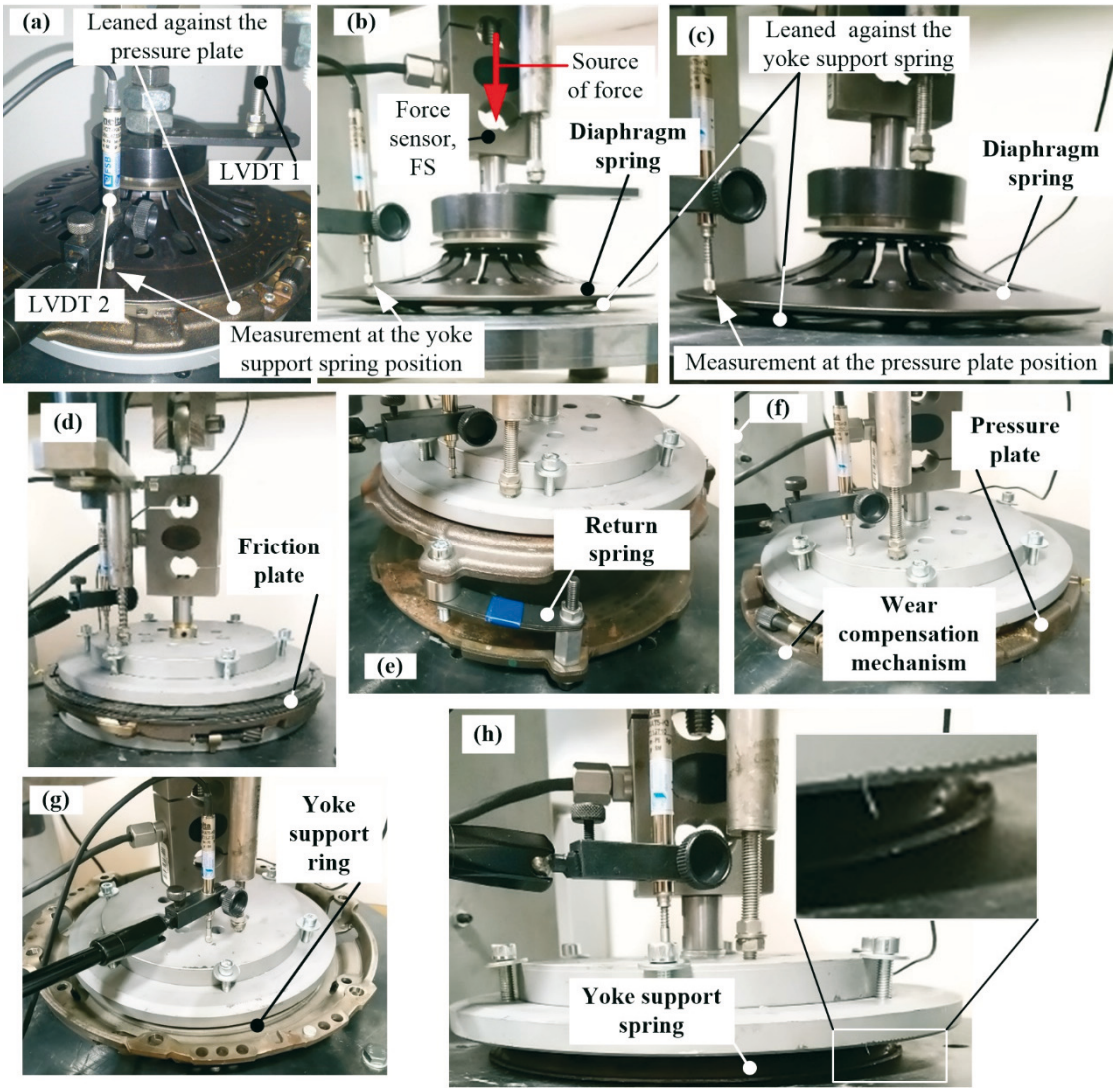

Fig. 8 Photographs of the characterization setups of individual components.

4.1 Diaphragm spring

On the actual clutch, the diaphragm spring leans against both the pressure plate and yoke support spring (see Fig. 2). For the sake of test implementation convenience, characterization was recorded for the cases when the diaphragm spring leans only against the pressure plate (Fig. 8a) or the yoke support spring (Fig. 8b-c). When the diaphragm spring leans against the pressure plate (Fig. 8a), the LVDT position sensor 2 measures the displacement at the yoke support spring position, while the deformation at the pressure plate positions is neglected. For the case (Fig. 8b-c), when the diaphragm spring leans against the yoke support spring, the experiments are recorded twice with LVDT 2 measuring the displacement either at the yoke support spring position (Fig. 8b) or at the pressure plate position (Fig. 8c). In addition to the two mentioned contact points, the contact point with the release bearing is also of interest and is measured by the LVDT position sensor 1. The obtained spring curves (Fig. 9a-c) were used to determine the diaphragm spring stress-strain characteristic for the newly proposed models, as presented in Section 5.

4.2 Friction plate

Friction plate compliance predominantly comes from the woven spring placed between the two friction discs to ensure uniform contact conditions during the clutch lock-up [4]. Similarity with the actual clutch assembly conditions is achieved by placing the friction plate between the original pressure plate and a solid steel disc representing the flywheel (Fig. 8d). The recorded stress-strain characteristic (Fig. 9d) shows the expected non-linear shape [17].

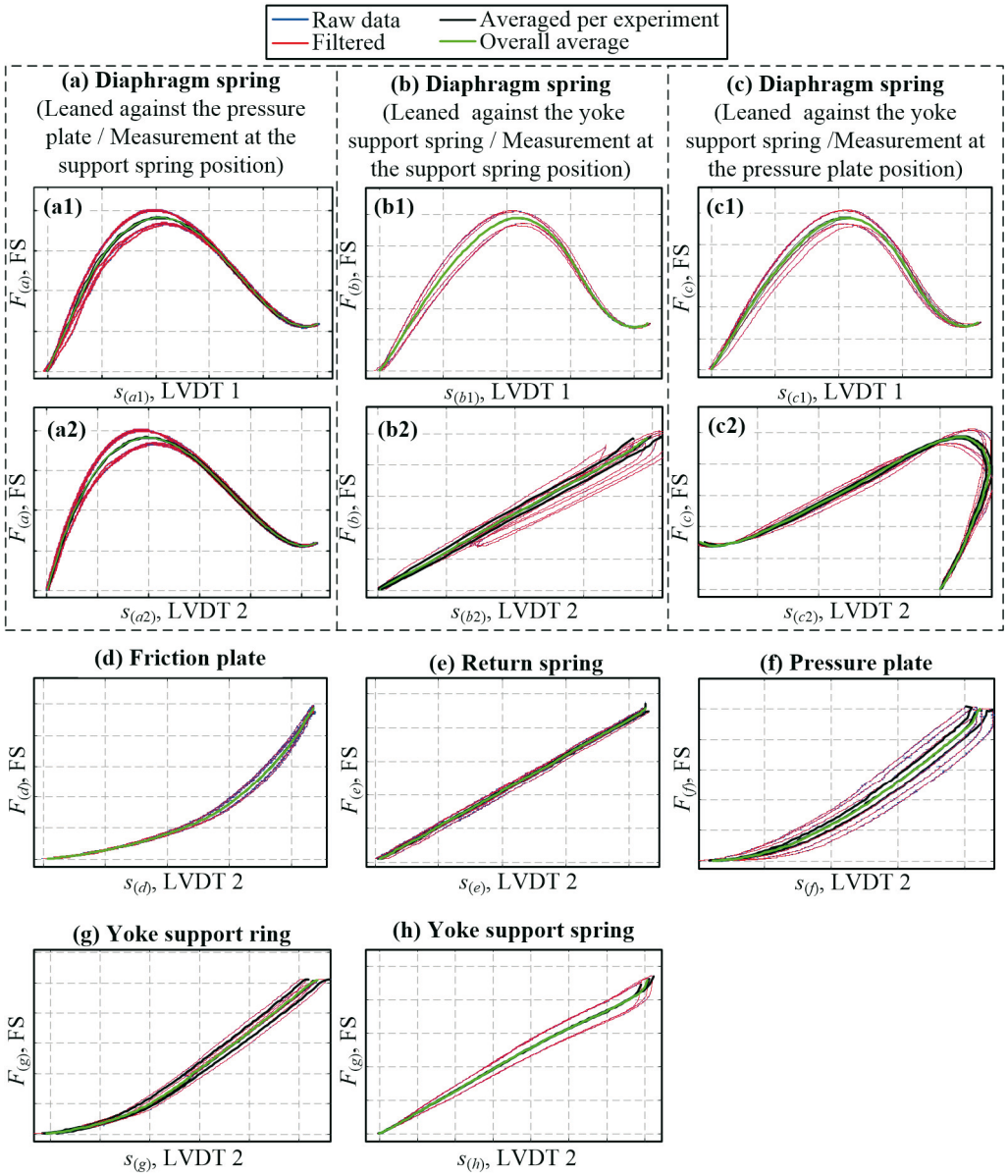

Fig. 9 Recorded stress-strain curves for axial dynamics of different clutch components.

4.3 Return spring

A multilayer leaf spring is used as a return spring. Textbooks, e.g. [18], typically provide equations that enable the calculation of the spring characteristic for a multilayer leaf spring for a set of parallel flat springs with hinge-type connections on both ends. Since the joints are here designed to be rigid, experimental characterization is the most reliable method to obtain the spring characteristic.

All three leaf springs were connected between two pressure plates (see Fig. 8e), thus placing the leaf springs in positions resembling the actual clutch conditions. The original rivets were replaced with screws and steel shells to maintain the initial distance between the press plates in order to enable sufficient disposition of the springs. The recorded characteristic (Fig. 9e) is approximately linear.

4.4 Pressure plate with a wear compensation mechanism

For the clutch type considered, the wear compensation mechanism, which is connected to the pressure plate (see illustration in Fig. 2), acts as an elastic support for the diaphragm spring lever. Due to the avoidance of individual wear compensation mechanism sub-models, the lumped characteristic was obtained by experimental characterization of the pressure plate and wear compensation mechanism assembled as on the actual clutch (see Fig. 8f). The recorded spring characteristic (Fig. 9f) is nonlinear and stiff.

4.5 Yoke support ring

The yoke support includes a solid steel ring placed within a circumferential groove on the yoke. The only source of elasticity is, thus, related to the deformation of the ring itself, and, compared to the other clutch components characterized, the ring is expected to have the highest stiffness. The spring characteristic of the support ring was characterized while placing it between two steel plates (Fig. 8g). This arrangement was chosen due to the significantly higher stiffness of the steel plates compared to the stiffness of the support ring. The obtained spring characteristic (Fig. 9g) is non-linear, with the note that in the actual clutch, the yoke support ring is pre-strained and will thus operate in the linear portion of the recorded characteristic.

4.6 Yoke support spring

The yoke support spring has a geometry similar to the diaphragm spring, and thus, the setup of the test rig for the yoke support spring (Fig. 8h) is similar to the one used for the diaphragm spring characterization. The obtained characteristic (Fig. 9h) is mildly non-linear with a mild stiffness.

5. Proposed models

Validation of the initially proposed model (Model 0; Section 3) showed that an improvement in the model quality can be achieved by more precise modelling of the elastic clutch components. Thus, four additional models (labelled as Models 1 to 4) are proposed in this section with different additional sources of elasticity. Functional schematics and bond graphs of the proposed models are presented in Figs. 10 and 11, respectively. The bond graph models have been converted to mathematical equations in a straightforward way and then implemented in Matlab Simulink. All friction losses are set to zero to enable a straightforward assessment of the modelling accuracy (no hysteresis appears in the characteristics). Each component was characterized starting from the released state while they were being pre-strained in the assembled clutch. The initial positions (pre-strains) of each component were determined from the inspection and measurements of the actual clutch.

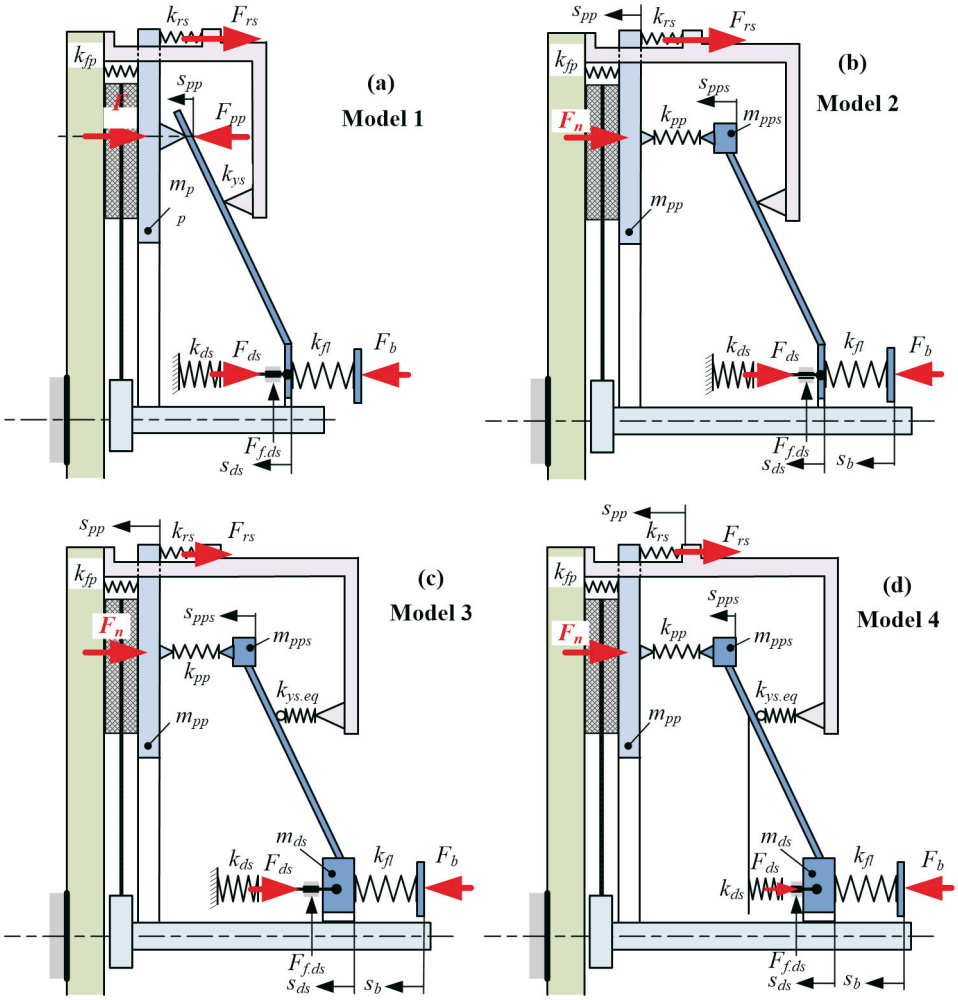

Fig. 10 Functional schematic of the proposed E-clutch models.

5.1 Model 1

Model 1 is based on Model 0 (cf. Fig. 11a and Fig. 5b) with the addition of compliance of the diaphragm spring levers (**C**:1/k_{fl}). The lever stiffness k_{fl} is calculated from the recorded characteristics from Figs. 9b and 9c:

$$k_{fl} = \frac{\Delta F_{ds}}{\Delta s_{b.ds} - i_{ds} \cdot \Delta s_{pp.ds}}, \tag{1}$$

where $F_{ds} = F_{(b)}$, $s_{b.ds} = s_{(b1)} - s_{(b2)}$, and $s_{pp.ds} = s_{(c2)} - s_{(b2)}$, i.e., displacements at the inner and outer edges of the diaphragm spring include the deformations of the support ring. Although the obtained lever stiffness turns out to be mildly varying (non-linear spring characteristic), the model was parameterized with a linearized, constant stiffness value. This constant value results in more consistent model validation results. The stress-strain characteristics of the diaphragm spring, friction plate, and return spring are implemented in the model as characterized, i.e., as shown in Figs. 9a1, 9d, and 9e, respectively.

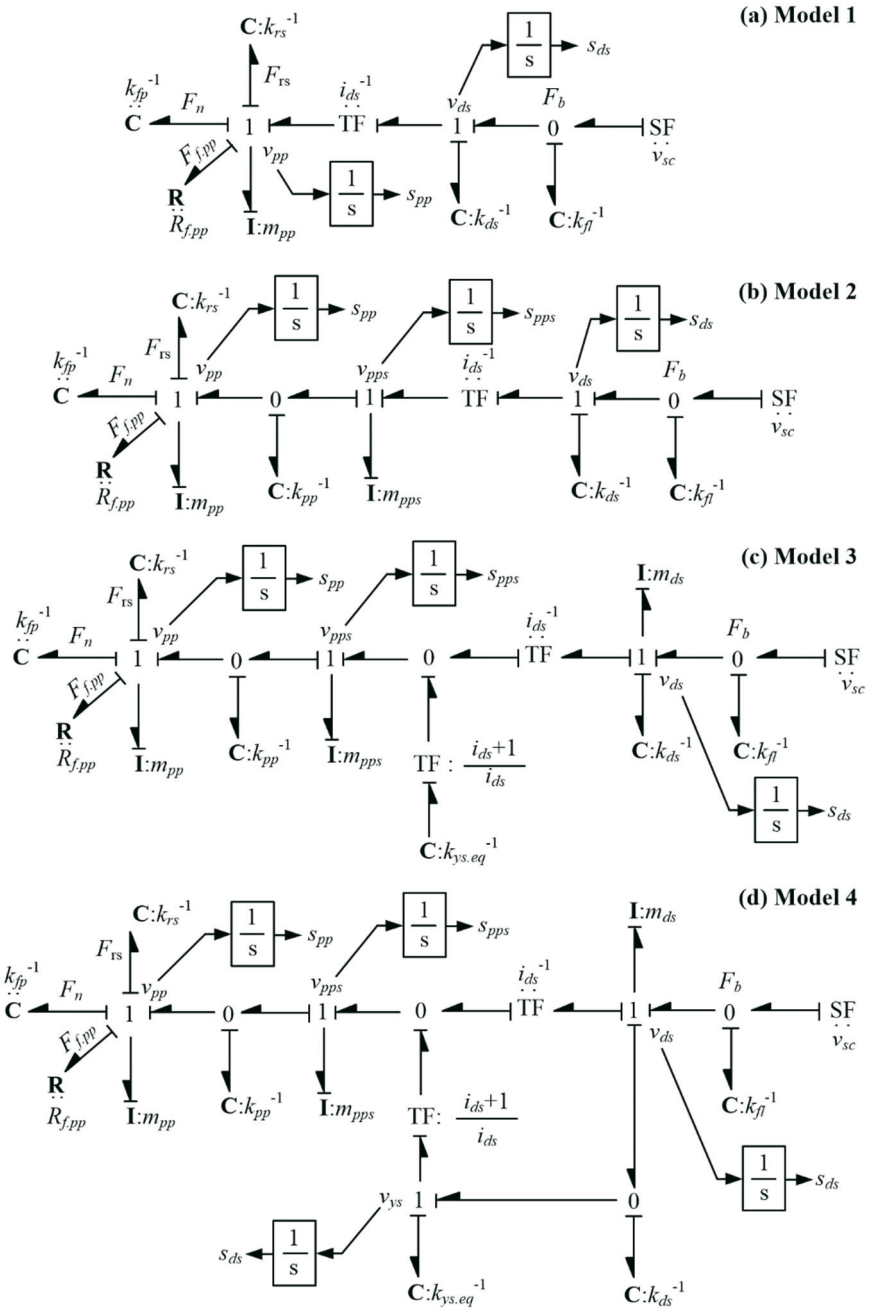

Fig. 11 Bond graphs of the proposed E-clutch models.

5.2 Model 2

Model 2 (Fig. 10b) is derived by extending Model 1 with the pressure plate spring characteristic (**C**:1/*kpp*) shown in Fig. 9f. In order to preserve the integral causalities, the bond graph model (Fig. 10b) is extended with an additional inertia element, which represents the mass of the diaphragm spring (**I**:*mpps*). Model validation provides the best results when the stiffness of diaphragm spring levers (*kfl*) is set to a constant value derived from the characterization results for the diaphragm spring placed against the pressure plate (Fig. 8a). Accordingly, the stiffness of the levers is again calculated using Eq. (1), but with recorded values shown in Fig. 8c, i.e., $F_{ds} = F_{(c)}$, $s_{b.ds} = s_{(c1)} - s_{(b2)}$, and $s_{pp.ds} = s_{(c2)} - s_{(b2)}$. Again, the obtained mildly non-linear characteristic is linearized.

5.3 Model 3

Model 2 is further extended by adding equivalent yoke support stiffness ($k_{ys.eq}$) calculated from the yoke support spring stiffness (kys, Fig. 9g) and the yoke support ring stiffness (k_{sr}, Fig. 9h) considered as serially connected mutually opposing springs. Again, additional inertia element (**I**: m_{ds}) is added (Fig. 11c) to preserve integral causalities. The diaphragm spring lever stiffness is adopted from Model 2. The equivalent yoke support stiffness is estimated by extrapolating the reconstructed curve **C**: $k_{ys.eq}$ because the operating range of the clutch is beyond the measurement range of the manual press test rig. The model validation results were improved by additionally increasing the stiffness of the yoke support $k_{ys.eq}$. It was reasoned that the reconstructed curve showed an unrealistically low stiffness because of a combination of the small displacement measured compared to the position sensor precision and the elasticity of the manual press test rig.

5.4 Model 4

Model 4 is based on Model 3 with the diaphragm spring placed towards the yoke support point rather than towards surroundings, which correlates with the actual positioning and relations between clutch components (cf. Figs. 10d and 10c). The correlation between the modelling and experimental results was found to be good if the stiffness values of the yoke support (**C**: $k_{ys.eq}$) and diaphragm spring (**C**:$1/k_{ds}$) were scaled by the factors of 20 and 1.3, respectively, compared to the characteristics used in Model 3. It was reasoned that this increase in stiffness compensated for the influence of measurement imprecision on the manual press rig due to its own compliance, whose influence is repeatedly introduced in the model with each added spring element.

6. Validation of the proposed models

Validation results related to all the proposed models are presented in Fig. 12. While the torque and release bearing positions were measured, the force on the release bearing (F_b) was calculated from the measured hydraulic fluid pressure (p) and slave bearing surface (A_{sl}) as $F_b = p\, A_{sl}$. The modelling precision evidently increases with each subsequent model, i.e., with each added physically realistic source of elasticity.

Model 1 shows a significant qualitative and quantitative improvement in the release bearing force prediction over Model 0 (Fig. 12a). The only noticeable difference between the prediction of Model 1 and experimental results exists around the release bearing force peak point (Fig. 12a), which correlates with the maximum clutch normal force and torque (Fig. 12b). In addition, the proposed models further improve the modelling accuracy in the "critical" (peak force) region, with Models 3 and particularly Model 4 being capable of describing the recorded force characteristic with significant precision. However, Model 3 shows reduced torque prediction accuracy compared to Model 4 and all the other models, which may be explained by the non-physical, fixed position of the diaphragm spring support. It may thus be concluded that Model 4 has the best overall prediction quality. One may argue that none of the models accurately predicts the stagnation in the force increase around the force peak. This may be explained by the absence of friction (i.e., stiction) in the models used in validation, which may become a more influential parameter for closed clutch conditions when the diaphragm spring generates maximum forces towards the supports and consequently the highest friction in the system.

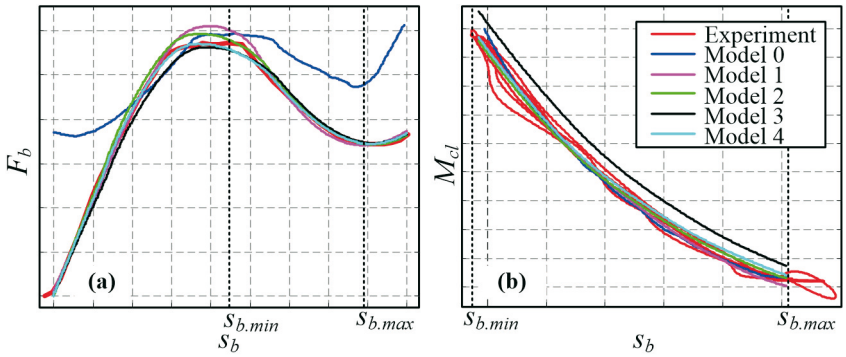

Fig. 12 Validation of the proposed models of clutch axial dynamics: a) Force on the release bearing vs. the release bearing position, b) Clutch torque vs. release bearing position.

7. Conclusion

The previously proposed simplified model of E-clutch axial dynamics has been gradually extended in four steps, resulting in four newly proposed lumped-parameter models. The model parameters include spring characteristics, masses, and friction. The spring characteristics of individual clutch components were experimentally characterized using a manually manipulated press rig. The masses of individual components were estimated based on known overall masses and the geometry of subcomponents. Friction was set to zero for the purpose of a straightforward assessment of the accuracy of static curves predicted by the proposed models.

All newly proposed models show a significant improvement in the prediction of force at the clutch release bearing. The fourth, most detailed model, shows the best prediction of both release bearing force and clutch torque compared to the other models presented and is therefore considered a good basis for future work.

Possibilities for additional improvements include: (i) inclusion of friction elements in the axial dynamics system model, which may further increase the modelling accuracy around the maximum release bearing force where friction (i.e., stiction) is expected to have the maximum influence; (ii) investigation into the possibility of reducing the model complexity by integrating several experimentally identified spring characteristics into a single, equivalent spring curve, and, consequently, omission of some individual mass (and friction) elements; and (iii) modelling of effects related to thermal expansion and wear processes (cf. [19] in the case of DCT clutch).

Acknowledgment

It is gratefully acknowledged that this study was supported by Ford Motor Company.

REFERENCES

[1] Tripathi K. A novel approach for enhancement of automobile clutch engagement quality using mechatronics based automated clutch system. J Inst Engrs India, Ser C 2013; 94: 9–20. https://doi.org/10.1007/s40032-013-0061-5

[2] Kimmig KL and Agner I. Double clutch – wet or dry, that is the question. In: 8th LuK symposium, Baden-Baden, Germany, 4–5 April 2006, pp. 119–135. Buhl: LuK.

[3] Berger R, Meinhard R and Bunder C. The parallel shift gearbox PSG – twin clutch gearbox with dry clutches. In: 7th LuK Symposium, Buhl, Germany, 11–12 April 2002, pp. 197–210. Buhl: LuK.

[4] Cappetti N, Pisaturo M and Senatore A. Modelling the cushion spring characteristic to enhance the automated dry-clutch performance: the temperature effect. Proc IMechE Part D: J Automobile Engineering 2012; 226(11): 1472–1482. https://doi.org/10.1177/0954407012445967

[5] Nouailletas R, Mendes E, Koenig D. Hybrid modelling and identification of dry friction systems, application to a clutch actuator, Control Engineering Practice18(2010)904–917. https://doi.org/10.1016/j.conengprac.2010.03.014

[6] Kroll J, Hausner M, Seebacher R. Mission CO2 Reduction - The future of the manual transmission, LuK Symposium 2014

[7] Vu, T.M.; Moezzi, R.; Cyrus, J.; Hlava, J.; Petru, M. Automatic Clutch Engagement Control for Parallel Hybrid Electric Vehicle. Energies 2021, 14, 7256. https://doi.org/10.3390/en14217256

[8] Machado FA, Kollmeyer PJ, Barroso DG, and Emadi A, Multi-Speed Gearboxes for Battery Electric Vehicles: Current Status and Future Trends, in IEEE Open Journal of Vehicular Technology, 2021, vol. 2, pp. 419-435, https://doi.org/10.1109/OJVT.2021.3124411

[9] Xi J; Si H, ; Gao J, Optimization of a Shift Control Strategy for Pure Electric Commercial Vehicles Based on Driving Intention, 2024, World Electr. Veh. J., 15, 44. https://doi.org/10.3390/wevj15020044

[10] Liu Y, Qin D, Jiang H, et al. Clutch torque formulation and calibration for dry dual clutch transmission. Mechanism and Machine Theory 2011; 46: 218-227. https://doi.org/10.1016/j.mechmachtheory.2010.09.005

[11] Vasca F, Iannelli L, Senatore A, et al. Modeling Torque Transmissibility for Automotive Dry Clutch Engagement. In: IEEE American Control Conference, Washington, (ed. Wayne Bequette), Seattle, USA, 11-13 June 2008, pp. 306-311, IEEE. https://doi.org/10.1109/ACC.2008.4586508

[12] Chen Z, Liu Y, Fu Y, et. al. Motor-torque-limited power-on upshift control in electric vehicles with automatic transmissions. Proc IMechE Part D, J Automobile Engineering, 2016; 230(1); 18-36. https://doi.org/10.1177/0954407015577309

[13] Hong S, Son H, Lee S, et. al. Shift control of a dry-type two-speed dual-clutch transmission for an electric vehicle. Proc IMechE Part D, J Automobile Engineering, 2016; 230(3); 308-321. https://doi.org/10.1177/0954407015585686

[14] Min G, Son H, Song M, et. al. Development of a gear fork control algorithm to improve the shift quality of a dual-clutch transmission. Proc IMechE Part D, J Automobile Engineering, 2016; 230(11); 1477-1487. https://doi.org/10.1177/0954407015613266

[15] Hoić M, Hrgetić, M, Deur J, Tissot, A. Design of a test rig in support of E-clutch dynamics characterization, modelling, and control, Powertrain Modelling and Control Conference PMC 2018, Loughborough, UK, 2018.

[16] Škugor B., Deur J., Ivanović V.; E-Clutch Torque Control Including Compensation of Thermal Expansion Effects, IEEE Transactions on vehicular technology, 2020, 69(1). https://doi.org/10.1109/TVT.2019.2953148

[17] Hoić M, Kranjčević N, and Deur J.; Experimental characterization of dry dual clutch elastic components with application to clutch modelling, International conference on powertrain modelling and control, Bradford, West Yorkshire, UK, 10–12 September 2014, Bradford: School of Engineering, Design and Technology, University of Bradford.

[18] Wahl AM. Mechanical Springs. 2nd ed. New York: McGraw-Hill, 1963, ISBN 978-0070677050

[19] Hoić M, Kranjčević N, Herold Z, Deur J, Ivanović V. Modeling of dry dual-clutch axial dynamics. Proceedings of the Institution of Mechanical Engineers, Part D: Journal of Automobile Engineering, 2018, 232(2), 220–237. https://doi.org/10.1177/0954407017694964.

Submitted: 30.8.2023

Accepted: 25.3.2024

Krunoslav Haramina
Nenad Kranjčević
Matija Hoić*
Joško Deur
University of Zagreb, Faculty of Mechanical Engineering and Naval Architecture, Zagreb, Croatia
Andreas Tissot
Ford-Werke GmbH, Cologne, North Rhine-Westphalia, Germany
*Corresponding author:
Matija.hoic@fsb.unizg.hr